Microscopy of terahertz spoof surface plasmons propagating on planar metamaterial waveguides

N. Sulollari,[1] S. J. Park,[2] M. Salih,[1] P. Rubino,[1] A. D. Burnett,[1] L. Li,[1] E. H. Linfield,[1] A. G. Davies,[1] J. E. Cunningham,[1] and P. Dean[1]

[1)] *School of Electronic and Electrical Engineering, University of Leeds, LS2 9JT, Leeds, United Kingdom*

[2)] *School of Electronic Engineering and Computer Science, Queen Mary University of London, E1 4NS, London, United Kingdom*

(*Electronic mail: P.Dean@leeds.ac.uk)

(Dated: 8 February 2024)

Surface plasmon polaritons (SPPs) are electromagnetic waves that have attracted significant interest owing to their subwavelength confinement and the strong field enhancement that they provide. Yet in the terahertz (THz) frequency region of the spectrum, which is well below the plasma frequency of metals, these surface waves are characterised by extremely weak confinement that has severely limited their exploitation for information processing and sensing. One means to circumvent this limitation is through subwavelength structuring of a metallic surface, which can thereby be engineered to support the propagation of spoof surface plasmon polaritons (SSPPs) that closely mimic the properties of SPPs. In this work, we report the design and experimental characterisation of an ultra-thin metamaterial planar waveguide that supports SSPPs at THz frequencies. Finite-element method simulations are shown to predict the excitation of SSPPs on the surface of our devices under free-space illumination at 3.45 THz. We investigate these structures experimentally using THz scattering-type scanning near-field microscopy (THz-s-SNOM) to map directly the out-of-plane electric field associated with the propagation of SSPPs on the surface of the waveguides. Our work paves the way for future development of plasmonic integrated circuit technologies and components operating in the THz frequency band.

I. INTRODUCTION

Surface plasmon polaritons (SPPs) are electromagnetic waves that propagate at the interface between a metal and a dielectric material through coupling between delocalised electrons and the electromagnetic field. These surface waves have attracted significant interest since they permit subwavelength confinement and thus provide strong field enhancement[1]. In particular, there has been growing interest in the development of plasmonic circuit technology that offers a bridge between electronic and photonic devices for information processing and sensing[2], with potential applications including super-resolution imaging[3], high-density optical data storage[4], and bio-sensing[5]. SPPs are typically exploited at optical and UV frequencies which are close to the plasma frequencies of metals[6]. However, at lower frequencies such as in the terahertz (THz) region of the spectrum, metals resemble perfect electric conductors (PEC), resulting in extremely poor confinement of SPPs such that the electromagnetic field propagates as a weakly confined Sommerfeld-Zenneck surface wave[7]. Nevertheless, the ability to confine and control light at terahertz frequencies that offer unique opportunities for sensing in areas as diverse as bio-medicine[8], biological and chemical sensing[9–12], and industrial inspection[13] is highly desirable. This has led to the investigation of new ways to transfer the ability of SPPs to confine light tightly in deep subwavelength dimensions to these lower frequencies. In this respect, it has been shown that the addition of subwavelength corrugations to a metal surface produces an enhanced surface impedance, which can be exploited to support the propagation of surface-bound modes even in the limit of perfect conductivity[14], thereby mimicking properties of SPPs[15,16]. These waves are known as spoof surface plasmon polaritons (SSPPs) and their dispersion relation closely follows those of SPPs.

In the microwave and sub-millimetre frequency regimes the propagation of SSPPs have been demonstrated experimentally on subwavelength-corrugated metallic structures including helically grooved wires[17], periodic chains of domino structures[18,19], and periodic metallic cylinders[20]. Furthermore, nearly zero-thickness metal strips printed on flexible, ultra-thin dielectric films have been shown to support the propagation of planar surface plasmon (PSP) modes that adapt to the curvature of the surface[21]. This allows the design of flexible plasmonic circuits that can be bent, twisted, or folded. Recent advances in PSP circuitry on ultra-thin metal films have provided a wide range of planar waveguide devices operating in the microwave and millimetre-wave regions[22], including multi-band waveguides[23,24], broadband converters from guided waves to PSPs[25], ultra-wideband beam splitters[26], frequency selective devices[27], ultra-wideband and low-loss filters[28–30], on chip sub-terahertz SSPP transmission lines in CMOS[31], and SSPP amplifiers[32].

At higher frequencies around $\sim$ 1 THz, periodically patterned planar structures supporting localised[33,34] and propagating[22,26] SSPPs have been proposed theoretically. Furthermore, the propagation and guiding of SSPPs on metallic surfaces patterned with a two-dimensional array of subwavelength apertures has been demonstrated experimentally at frequencies up to $\sim$ 1.5 THz[35]. In this case the propagation of SSPP modes along the metallic surfaces was verified by transmission measurements accomplished using THz time-domain spectroscopy, although this approach is sensitive only to the macroscopic device properties and is insufficient to reveal insights into the light-matter interactions on the microscopic scale. To this end, there has been consider-

able interest in the application of techniques for visualising with sub-wavelength resolution the THz field supported on the surface of microscopic devices. Particularly, one approach that provides a nanometer-scale spatial resolution which is independent of the incident wavelength is scattering-type scanning near-field optical microscopy (s-SNOM)[36]. This technique has been successfully applied to the visualisation of plasmonic[37] and photonic[38] modes in individual THz resonators, as well as the nano-imaging of THz SSPPs in doped semiconductors[39] and THz Dirac plasmon polaritons in topological insulators[40,41].

In this work, we report the design and experimental characterisation of an ultra-thin metamaterial planar waveguide that supports SSPPs at THz frequencies. Finite-element method (FEM) simulations are shown to predict the excitation of SSPPs on the surface of our devices under free-space illumination by a narrowband beam at 3.45 THz. We furthermore investigate the use of grating couplers integrated on the waveguides to enhance the excitation of SSPPs. We investigate these structures experimentally through the use of THz-s-SNOM to map directly the out-of-plane electric field associated with the propagation of SSPPs on the surface of the waveguides, with deeply-subwavelength resolution. The experimental measurements under both $s-$ and $p-$polarised excitation show good agreement with simulations. Our work represents this first direct observation of propagating THz-frequency SSPPs on a planar waveguide and paves the way for the future development of plasmonic integrated circuit technology operating in this technologically important frequency range.

II. DESIGN OF PSP WAVEGUIDES

Our waveguide structure supporting SSPPs at THz frequencies is based on a plasmonic metamaterial consisting of an ultra-thin metallic comb structure supported by a rigid substrate, as depicted in Fig. 1 (inset). This design is adapted from Ref.[21] where experimental results were reported at microwave frequencies ($f = 10$ GHz). To support SSPPs at the target frequency > 3 THz, our structure is designed with a period $d = 7.5$ m which is treated as the unit length, and a duty-cycle $a/d = 0.733$, total width $w = 8$ m, stub length $h = 6$ m, and film thickness $t = 100$ nm. The metalisation used to form the plasmonic waveguide is gold and it is supported on a float-zone silicon substrate of thickness 500 m and with dielectric constant $\varepsilon_r = 11.65$ at frequency $f = 3.45$ THz, as determined experimentally from THz time-domain spectroscopy measurements (see Supplementary Information Fig. S1). The dispersion relation for the fundamental mode of the TM-polarised waves supported by the structure was calculated using the eigenmode solver in ANSYS HFSS, in which a unit cell of the waveguide was considered with periodic boundaries in the $x-$direction and PEC boundaries in the $y-$direction. As can be seen in Fig. 1, the dispersion relation deviates significantly from the light line, indicating that the waveguide supports the propagation of confined modes. The SSPP wavelength is related to the SSPP wave-vector according to the relation $\lambda_{SP} = 2\pi/k_x$, which yields a value of $\lambda_{SP} = 18.5$ m at the target frequency 3.45 THz.

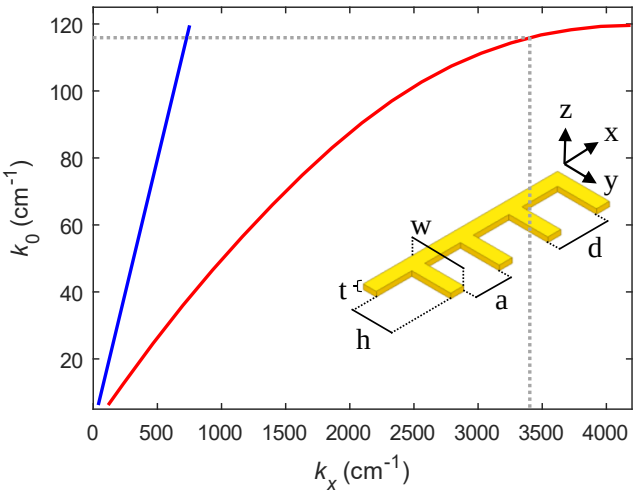

FIG. 1. Dispersion relation of the of the fundamental SSPP mode of the waveguide structure (red) and light line (blue). The dashed lines indicate the incident wavevector $k_0 = 1/\lambda_0$ (cm^{-1}) and SSPP wavevector, k_x, for the case $f_0 = 3.45$ THz. (inset) Geometric parameters of the designed structure, for which $w = 1.07d$, $a = 0.733d$, and $h = 0.8d$, where $d = 7.5$ m.

To analyse the propagation of SSPPs along the structure, simulations were performed for a finite waveguide, consisting of 27 repetitions of the unit cell, corresponding to a total length, $L = 208$ m, which was excited using a waveport positioned at $x = 0$ and polarised along the $z-$direction. Figure 2 (a) shows the out-of-plane field E_z obtained in the $x-y$ plane on the waveguide surface for an excitation frequency 3.45 THz. The field can be seen to oscillate periodically and also decay along the waveguide axis, which is a characteristic of a SSPP propagating in the $x-$direction. To quantify this behaviour further, the field amplitude was spatially averaged within each stub (of length $h = 6$ m and width $d - a = 2$ m) and plotted as a function of distance along the waveguide, as shown in Fig. 2 (b). To a good approximation the propagating SSPPs can be modelled as a wave bound to the surface of the metallic waveguide with an out-of-plane field given by the complex amplitude

$$E_z = E_0 \exp\left[-i(k_x x - \theta) - \frac{x}{L_p}\right] \qquad (1)$$

in which, E_0 is the amplitude, which is dependent on the excitation field, k_x is the wave-vector, θ is the phase relative to the excitation field, and L_p is the finite propagation length which depends on the finite conductivity of the metal. A numerical fitting of the simulated field values to Eq. 1 is shown in Fig. 2 (b), from which the wave-vector $k_x = 3400$ cm^{-1} is obtained, in agreement with the value obtained from the dispersion relation shown in Fig. 1. In addition, a propagation length $L_p = 75$ m is determined from the fit, in agreement with the S-parameters calculated for this finite waveguide (see Supplementary Information Fig. S2). The small discrepancy between the values of L_p obtained from the two approaches can

be explained by the electric field within each stub not being uniformly distributed. As such, the data points in Fig. 2 (b) do not fully capture the same level of detail as the S_{21} parameter calculation, but nevertheless serve as a reliable means of reducing the two-dimensional simulations to a one-dimensional analytical model.

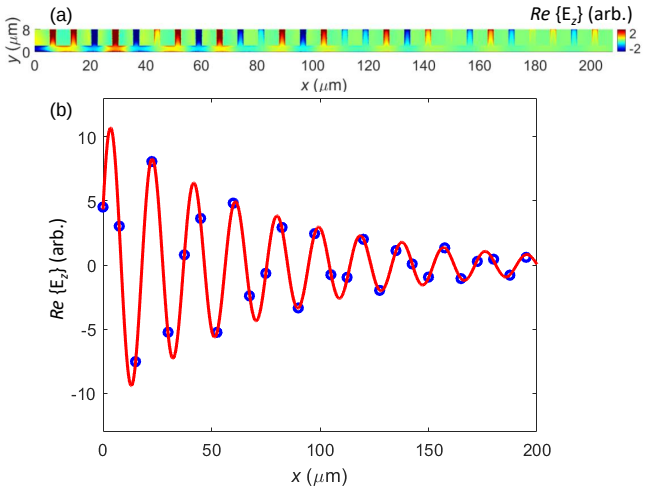

FIG. 2. (a) Simulated real part of the out-of-plane field E_z on the surface of the waveguide when excited by an excitation part at $x = 0$. (b) Spatially-averaged value of field plotted as a function of distance along the waveguide axis (blue circles) along with numerical fitting to Eq. 1 (red line). The values of the fitting parameters are: $E_0 = 11$ (a.u.), k_x = 3400 cm^{-1}, $\theta = 1.2$ rad, and $L_p = 75$ m.

In the case of free-space excitation of SSPPs on the waveguide, the momentum mismatch between the incident beam and the subwavelength SSPPs should be considered. Simulations have confirmed this momentum mismatch can be addressed by exploiting diffraction of the free-space beam at the edge of our waveguide structure, whereby components of the diffracted light whose wave-vector coincides with the SSPP wave-vector can couple to surface polaritons (see Supplementary Information Fig. S3 and S4). Nevertheless, to improve the coupling of an obliquely-incident beam to SSPPs further, we have employed an integrated grating structure as shown in Fig. 3 (a). The coupling efficiency of light to SSPPs on the waveguide depends primarily on the grating period, α, but also on the grating duty-cycle β, the width w_s of the grating apertures, and the total length of the grating structure, L_g. Through variation of these parameters in FEM simulations we have determined, for the illumination geometry corresponding to our experimental system, an optimum grating period of $\alpha = 23$ m in the case when $\beta = 50\%$, $w_s = 25$ m, and $L_g \approx \lambda_0 = 87$ m (see Supplementary Information Fig. S5 and S6).

III. RESULTS AND DISCUSSION

In order to confirm the excitation of SSPPs on our structures and to investigate their properties experimentally, we have employed THz-s-SNOM to map the spatial distribution of the out-of-plane field on the surface of the waveguides. The s-SNOM system employs a 3.45-THz quantum cascade laser (QCL) as both excitation source and coherent receiver by exploiting the laser self-mixing effect, as described elsewhere[37]. The QCL was cooled using a continuous-flow liquid–He cryostat and maintained at a heat sink temperature of 20 0.01 K. A current source was used to drive the laser with a dc current of 420 mA and emission from the QCL was focused to the $\sim$ 20 nm apex of a vertically aligned near-field microscope probe positioned in the near-field of the sample surface, at an incident angle of $\sim 54^{\circ}$ to the surface normal. Radiation scattered to the far-field by the probe was coupled back to the QCL along the same optical path as the incident beam and reinjected to the laser cavity. To isolate the signal component arising from the near-field interaction between the probe and the sample, the microscope probe was operated in tapping mode and the QCL terminal voltage was amplified using an ac-coupled low-noise voltage amplifier and then demodulated at harmonics of the probe tip's tapping frequency ($\Omega \sim 80$ kHz) using a lock-in amplifier. The tapping amplitude was $A_{tip} \approx 200$ nm, and the time constant used was $\tau_s = 50$ ms. Under these experimental conditions the feedback parameter has been measured to be $C \sim 0.1$ and the noise equivalent power of the self-mixing detection scheme is estimated to be ~ 3 pW.

Our FEM simulations have shown that SSPPs may be excited on our structures using an obliquely incident free-space beam with either $p-$ or $s-$polarisation (see Supplementary Information). We initially study the excitation of SSPPs using a $p-$polarised beam obliquely incident on the waveguide as shown in Fig. 3 (b). In this case, a grating structure with period $\alpha = 20$ m was integrated on the end of the waveguide with the other end left unmodified. Samples were fabricated on a float zone silicon substrate of thickness 500 m with 5 nm/100 nm metallic layers of Ti/Au defined by optical lithography and thermal evaporation. The topography of a section of the fabricated sample obtained by AFM is shown in Fig. 3 (c). Figure 3 (d) shows the spatial distribution of the $n = 2$ harmonic of the self-mixing voltage, V_{SM} measured using THz-s-SNOM with a pixel size 250 nm $\times$ 250 nm. It has been shown previously[37] that the image contrast in THz-s-SNOM comprises contributions from two distinct components. The first of these, with magnitude s_ε and phase ϕ_ε, is principally excited by $p-$polarised components of the incident THz field and arises from the near-field dipole interaction between illuminated tip and sample surface, thereby capturing information about the local permittivity of the sample. In contrast, the second term with magnitude s_z and phase ϕ_z, is mostly insensitive to the bulk material properties but captures the spatial distribution of the out-of-plane field E_z supported by the sample under excitation by the incident field. The SM signal can then be expressed in terms of the individual signal contributions corresponding to the respective scattering terms according to

$$V_{SM} = s_\varepsilon + s_z e^{-i\phi_z}. \quad (2)$$

Here, the approximation $\phi_\varepsilon \approx 0$ has been applied, as is ex-

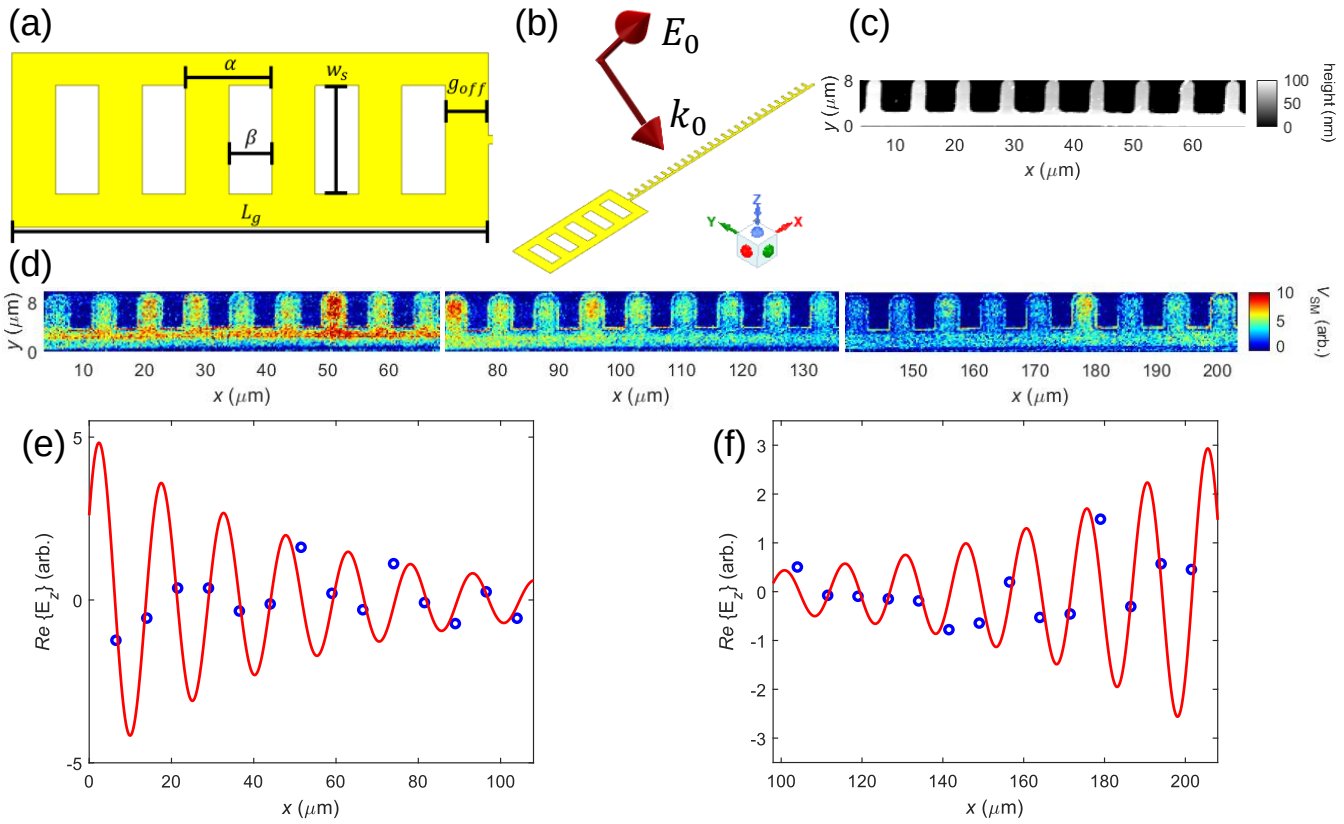

FIG. 3. (a) Schematic diagram showing the geometry of the grating structure. (b) Schematic diagram illustrating integration of the grating on a waveguide of length $L = 208$ m, as well as the beam propagation direction and field polarisation of the obliquely-incident THz beam used in the experiments. The incident beam propagates in the $y-z$ plane and is also $p-$polarised in this plane. (c) AFM image of a section the fabricated waveguide. (d) Terahertz image of the sample obtained by s-SNOM, in which the signal is derived from the $n = 2$ harmonic of the self-mixing voltage. (e) Spatially-averaged value of field plotted as a function of distance along the waveguide axis in the range $x = 0 - 104$ m and (f) $x = 104 - 208$ m (blue circles) along with the numerical fits to Eq. 1 (red lines). The fitted values of θ here depend on the phase of the SSPP wave relative to the excitation field, as well as the path length between the QCL facet and the s-SNOM tip in the experimental system.

pected for radiation frequencies far away from any phonon or bulk plasmonic material resonances[37,42]. Furthermore the magnitude s_ε is expected to be spatially constant along the waveguide structure, and can be readily estimated from the spatial average of the signal recorded across all metallic regions of the sample. Using Eq. 2 this term can thereby be subtracted from the measured signal to isolate the signal $s_z e^{-i\phi_z}$ in each image pixel. It is important to note that the out-of-plane field E_z quantified by this signal may itself contain contributions from not only the SSPP mode supported by the waveguide but also the charge distribution induced directly by the obliquely incident THz field, whereby the stubs of our waveguide structure behave as electrically-short dipoles. This charge distribution is dependent on the polarisation of the incident field (see Supplementary Information Figs. S3 and S4) and its affect can be treated to a reasonable approximation as causing a constant offset to the out-of-plane field when spatially-averaged within each stub of the waveguide.

Figures 3 (e) and 3(f) show the values of $Re(s_z e^{-i\phi_z})$ obtained in this way following spatial averaging over 192 pixels within each stub of the waveguide and subtraction of the constant offset described above. Since the waveguide length $L = 208$ m is greater than the expected propagation length of SSPPs on this structure we assume negligible interaction between SSPPs launched from opposite ends, and therefore analyse SSPPs on each half of the waveguide independently. Figures 3(e) and 3(f) show the resulting fits of the data to Eq. 1, from which the estimates $k_x = 4180 \pm 360$ cm^{-1} and $L_p = 51 \pm 30$ m are obtained. The large relative uncertainties in these values arise from the low sampling resolution along the $x-$direction. Notably this fitted value of the wave-vector is greater than that obtained from the eigen-mode simulations ($k_x = 3400$ cm^{-1}), which itself is congruous with values obtained from FEM simulations under plane wave illumination (see Supplementary Information). One possible explanation for this is the influence of the probe tip in the near-field of the sample, which is not accounted for in our simulations. Indeed, it is well known that the process of measurement in s-SNOM can result in modification of photonic modes supported by nanophotonic systems[43,44], owing to the near-field interaction between the tip and the sample. Additionally, the charge distribution induced directly on the surface of the waveguide by the obliquely incident THz field may cause departures from the simple model for the out-of-plane field described by Eq.

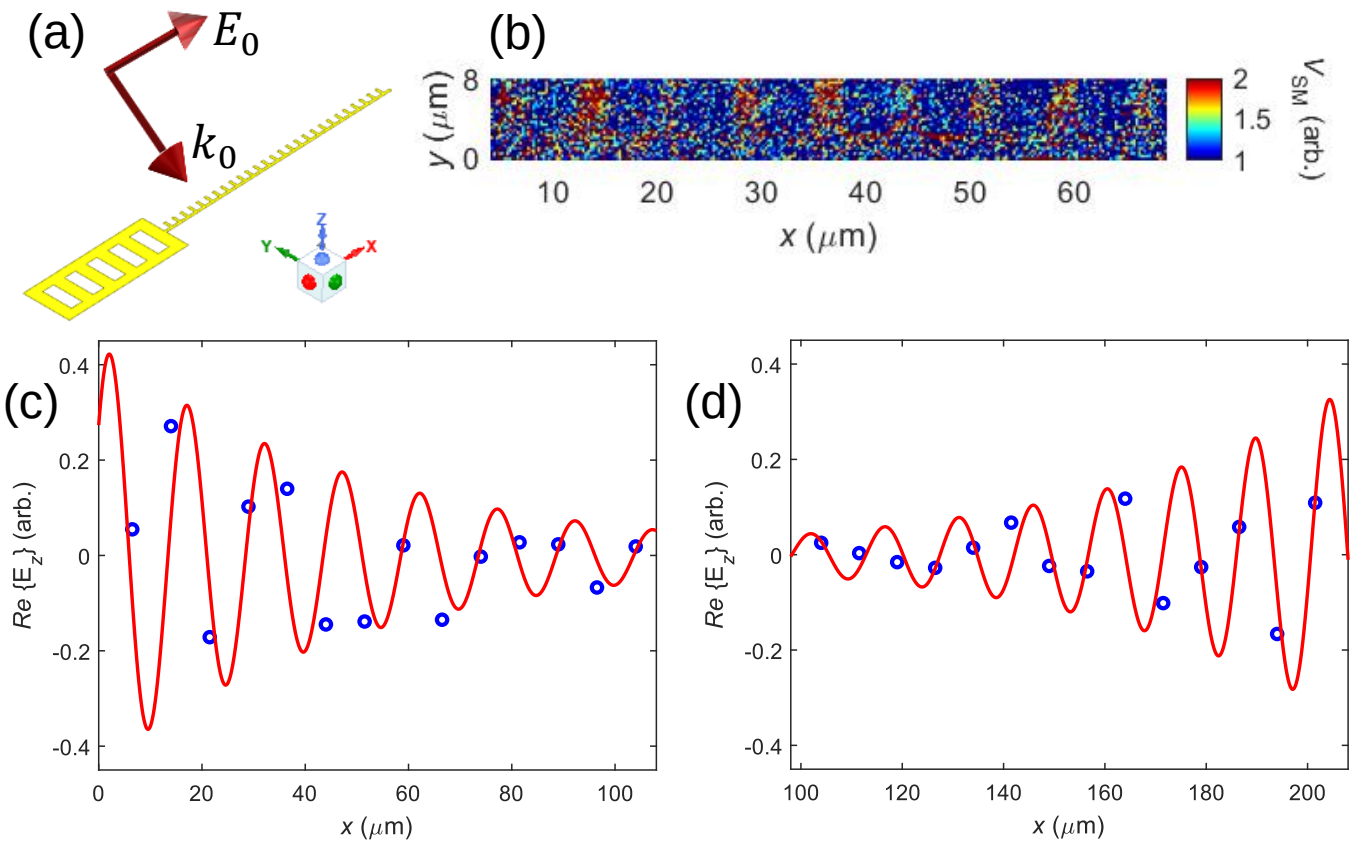

FIG. 4. (a) Schematic diagram showing the beam propagation direction and field polarisation of the obliquely-incident THz beam. The incident beam propagates in the $y-z$ plane and is $s-$polarised along the $x-$direction. (b) Terahertz image of the sample obtained by s-SNOM, in which the signal is derived from the $n=2$ harmonic of the self-mixing voltage. (c) Spatially-averaged value of field plotted as a function of distance along the waveguide axis in the range $x=0-104$ m and (d) $x=104-208$ m (blue circles) along with the numerical fits to Eq. 1 (red lines).

1. Another possible explanation for the observed discrepancy are slight differences between the dimensions of the experimental samples and the ideal designs used in the simulations, which can occur owing to edge-roughness/blurring in the optical lithography process used. Nevertheless we note reasonable agreement between the value of L_p obtained experimentally and from simulations. Finally, from the data in Fig. 3 we can compare the amplitude of SSPPs launched from the grating structure (shown in Fig. 3(e)) with those launched from the unmodified end of the waveguide (shown in Fig. 3(f)). We find the former, for which the fitted value $E_0=5.1\pm3.2$ a.u. is obtained, to be slightly larger than the latter, for which the value $E_0=3.1\pm1.7$ a.u. is obtained from the fitting procedure. The ratio of these values $\gamma\approx1.6$ indicates our integrated grating structure is effective at improving the coupling of the obliquely-incident beam to SSPPs on the waveguide, in agreement with predictions from simulation which yield $\gamma\approx1.5$. However we note the large uncertainties on these experimental values, which arise from the reduced sampling resolution along the x-direction, make an accurate quantitative comparison difficult.

When the incident beam is $p-$polarised as above, $z-$components of the radiation field will interact strongly with the vertically-aligned s-SNOM tip. Due to the strong confinement effect at the tip apex a non-negligible component of the photon momentum is thereby generated at the SSPP wavevector, which can launch SSPPs in the near-field of the tip[45]. In order to circumvent this possibility we also investigate the direct excitation of SSPPs on our waveguide structures using an $s-$polarised incident beam as shown in Fig. 4 (a). To this end, we have employed a quartz zero-order half-wave plate (HWP), positioned in the beam path between the QCL and the near-field probe, to control the incident polarization state in our system. As shown elsewhere[37], the p-polarised field scattered from the tip may still generate a small but measurable SM voltage signal owing to a small but non-negligible component of circularly polarized light in the QCL radiation field. Figure 4 (b) shows the spatial distribution of this signal obtained by THz-s-SNOM from a waveguide incorporating a grating structure of period $\alpha=23$ m. The corresponding values of $Re(s_z e^{-i\phi_z})$ obtained from the signal spatially averaged within each stub of the waveguide, following subtraction of the dipole interaction term in Eq. 2, are shown in Fig. 4 (c) and 4 (d). As before, SSPPs are seen to be launched from each end of the waveguide, characterised by an oscillatory out-of-plane field that decays as the SSPPs propagate along the waveguide axis. To quantify the amplitudes of the SSPPs launched from each end of the waveguide, we again fit the ex-

perimental values to Eq. 1, using the previously determined parameters, $k_x = 4180\ \mathrm{cm}^{-1}$ and $L_p = 51$ m. These fits, shown in Fig. 4 (c) and 4 (d), yield the values $E_0 = 0.4 \pm 0.3$ a.u. for the end of the waveguide incorporating the grating, and $E_0 = 0.3 \pm 0.1$ a.u. for the unmodified waveguide. From the ratio of these values $\gamma \approx 1.3$, which also agrees with the value $\gamma \approx 1.5$ obtained from simulations, it can again be concluded that the grating structure is effective at improving the coupling of the $s-$polarised beam to SSPPs on the waveguide. It should also be noted that these values being considerably smaller than those obtained under $p-$polarised excitation does not indicate a weaker out-of-plane field associated with SSPPs under $s-$polarised excitation, but rather this is due to much weaker mixing between the orthogonal polarisation states of the incident and scattered fields in this case.

IV. CONCLUSION

To conclude, we have presented the design, simulation, and experimental demonstration of an ultra-thin metamaterial planar waveguide that supports spoof surface plasmon polaritons at THz frequencies. We have furthermore successfully mapped with deeply subwavelength resolution the spatial distribution of the electric field associated with SSPPs propagating on such waveguides for the first time. Our results confirm excitation of SSPPs on these structures under both $p-$polarised and $s-$polarised excitation by a free-space beam at 3.45 THz. We have also shown that grating structures integrated on the waveguide can be used to enhance the coupling of light to SSPPs on the waveguides. Our work paves the way for future development of plasmonic integrated circuit technologies and components operating in the THz frequency band, including for example transmission lines, beamsplitters, frequency selective devices, multiplexers, and ultrawideband and low-loss filters. Future possible research directions include the development of conformal THz waveguides printed on flexible films which can be bent or twisted[21], or active devices whereby the transmission of SSPPs along the waveguide can be controlled electronically.

AUTHORS' CONTRIBUTIONS

P.D. and N.S. conceived the idea, developed the experimental setup, and performed the measurements. Waveguide structures were designed by N.S. and simulations were performed by N.S and S.J.P. Structures were fabricated by N.S. and M.S. Measurements of the dielectric constant of silicon as a function of frequency were acquired by A.D.B. Data were analyzed by N.S. with support from P.D. and J.E.C. The QCL structure was grown by L.L. under the supervision of E.H.L. Devices were processed by P.R. under the supervision of E.H.L and A.G.D. The manuscript was written by N.S., P.D. and J.E.C. with contributions from all the authors.

SUPPLEMENTARY MATERIAL

The supplementary material show the dielectric constant of silicon as a function of frequency measured using THz-TDS. The S_{21} parameter of the waveguide structure is shown, calculated using ANSYS HFSS for a waveguide with total length $L = 73$ m. The simulation of the waveguides under illumination by a free-space beam and the optimisation of grating parameters are also shown for the cases of $p-$polarised and $s-$polarised excitations, according to the geometries shown in Fig. 3 (b), and in Fig. 4 (a) respectively. Approach curves obtained from the $n = 1-5$ harmonics of the demodulated self-mixing voltage signal in THz-s-SNOM are also shown.

ACKNOWLEDGMENTS

The authors acknowledge support from EPSRC (UK) Programme grants 'HyperTerahertz' (EP/P021859/1) and 'Teracom' (EP/W028921/1), EPSRC grant EP/V004743/1, the Royal Society, and the Wolfson Foundation (grants WM110032, WM150029).

DATA AVAILABILITY STATEMENT

The data utilized in the development of this article can be found at: `https://doi.org/10.5518/1456`

REFERENCES

[1] W. L. Barnes, A. Dereux, and T. W. Ebbesen, "Surface plasmon subwavelength optics," Nature **424**, 824 (2003).
[2] E. Ozbay, "Plasmonics: Merging photonics and electronics at nanoscale dimensions," Science **311**, 189–193 (2006), https://www.science.org/doi/pdf/10.1126/science.1114849.
[3] X. Zhang and Z. Liu, "Superlenses to overcome the diffraction limit," Nature Materials **7**, 435–441 (2008).
[4] C. Genet and T. W. Ebbesen, "Light in tiny holes," Nature **445**, 39–46 (2007).
[5] S. Nie and S. R. Emory, "Probing single molecules and single nanoparticles by surface-enhanced raman scattering," science **275**, 1102–1106 (1997).
[6] T.-I. Jeon and D. Grischkowsky, "Thz zenneck surface wave (thz surface plasmon) propagation on a metal sheet," Applied physics letters **88** (2006).
[7] K. Wang and D. M. Mittleman, "Metal wires for terahertz wave guiding," Nature **432**, 376–379 (2004).
[8] V. P. Wallace, A. Fitzgerald, S. Shankar, N. Flanagan, R. Pye, J. Cluff, and D. Arnone, "Terahertz pulsed imaging of basal cell carcinoma ex vivo and in vivo," British Journal of Dermatology **151**, 424–432 (2004).
[9] D. J. Cook, B. K. Decker, G. Dadusc, and M. G. Allen, "Through-container thz sensing: applications for biodetection," in *Chemical and Biological Standoff Detection*, Vol. 5268 (SPIE, 2004) pp. 36–42.
[10] K. Kawase, Y. Ogawa, Y. Watanabe, and H. Inoue, "Non-destructive terahertz imaging of illicit drugs using spectral fingerprints," Optics express **11**, 2549–2554 (2003).
[11] M. Lu, J. Shen, N. Li, Y. Zhang, C. Zhang, L. Liang, and X. Xu, "Detection and identification of illicit drugs using terahertz imaging," Journal of Applied Physics **100** (2006).
[12] Y. Shen, a. T. Lo, P. Taday, B. Cole, W. Tribe, and M. Kemp, "Detection and identification of explosives using terahertz pulsed spectroscopic imaging," Applied physics letters **86** (2005).

[13]N. Karpowicz, H. Zhong, C. Zhang, K.-I. Lin, J.-S. Hwang, J. Xu, and X.-C. Zhang, "Compact continuous-wave subterahertz system for inspection applications," Applied Physics Letters **86** (2005).
[14]J. Pendry, L. Martin-Moreno, and F. Garcia-Vidal, "Mimicking surface plasmons with structured surfaces," science **305**, 847–848 (2004).
[15]G. Goubau, "Surface waves and their application to transmission lines," Journal of Applied Physics **21**, 1119–1128 (1950).
[16]D. Mills and A. Maradudin, "Surface corrugation and surface-polariton binding in the infrared frequency range," Physical Review B **39**, 1569 (1989).
[17]A. Fernández-Domínguez, C. R. Williams, F. García-Vidal, L. Martín-Moreno, S. R. Andrews, and S. Maier, "Terahertz surface plasmon polaritons on a helically grooved wire," Applied Physics Letters **93** (2008).
[18]E. M. Brock, E. Hendry, and A. P. Hibbins, "Subwavelength lateral confinement of microwave surface waves," Applied Physics Letters **99** (2011).
[19]Y. Zhang, Y. Xu, C. Tian, Q. Xu, X. Zhang, Y. Li, X. Zhang, J. Han, and W. Zhang, "Terahertz spoof surface-plasmon-polariton subwavelength waveguide," Photonics Research **6**, 18–23 (2018).
[20]Y. Zhang, S. Li, Q. Xu, C. Tian, J. Gu, Y. Li, Z. Tian, C. Ouyang, J. Han, and W. Zhang, "Terahertz surface plasmon polariton waveguiding with periodic metallic cylinders," Opt. Express **25**, 14397–14405 (2017).
[21]X. Shen, T. J. Cui, D. Martin-Cano, and F. J. Garcia-Vidal, "Conformal surface plasmons propagating on ultrathin and flexible films," Proceedings of the National Academy of Sciences **110**, 40–45 (2013).
[22]X. Liu, Y. Feng, K. Chen, B. Zhu, J. Zhao, and T. Jiang, "Planar surface plasmonic waveguide devices based on symmetric corrugated thin film structures," Optics express **22**, 20107–20116 (2014).
[23]X. Gao, J. Hui Shi, X. Shen, H. Feng Ma, W. Xiang Jiang, L. Li, and T. Jun Cui, "Ultrathin dual-band surface plasmonic polariton waveguide and frequency splitter in microwave frequencies," Applied Physics Letters **102** (2013).
[24]X. Liu, Y. Feng, B. Zhu, J. Zhao, and T. Jiang, "High-order modes of spoof surface plasmonic wave transmission on thin metal film structure," Optics Express **21**, 31155–31165 (2013).
[25]H. F. Ma, X. Shen, Q. Cheng, W. X. Jiang, and T. J. Cui, "Broadband and high-efficiency conversion from guided waves to spoof surface plasmon polaritons," Laser & photonics reviews **8**, 146–151 (2014).
[26]X. Gao, L. Zhou, X. Y. Yu, W. P. Cao, H. O. Li, H. F. Ma, and T. J. Cui, "Ultra-wideband surface plasmonic y-splitter," Optics express **23**, 23270–23277 (2015).
[27]J. Y. Yin, J. Ren, H. C. Zhang, B. C. Pan, and T. J. Cui, "Broadband frequency-selective spoof surface plasmon polaritons on ultrathin metallic structure," Scientific reports **5**, 8165 (2015).
[28]X. Gao, L. Zhou, Z. Liao, H. F. Ma, and T. J. Cui, "An ultra-wideband surface plasmonic filter in microwave frequency," Applied Physics Letters **104** (2014).
[29]Q. Zhang, H. C. Zhang, J. Y. Yin, B. C. Pan, and T. J. Cui, "A series of compact rejection filters based on the interaction between spoof spps and csrrs," Scientific Reports **6**, 28256 (2016).
[30]J. Xu, Z. Li, L. Liu, C. Chen, B. Xu, P. Ning, and C. Gu, "Low-pass plasmonic filter and its miniaturization based on spoof surface plasmon polaritons," Optics Communications **372**, 155–159 (2016).
[31]Y. Liang, H. Yu, H. C. Zhang, C. Yang, and T. J. Cui, "On-chip subterahertz surface plasmon polariton transmission lines in cmos," Scientific reports **5**, 14853 (2015).
[32]H. C. Zhang, S. Liu, X. Shen, L. H. Chen, L. Li, and T. J. Cui, "Broadband amplification of spoof surface plasmon polaritons at microwave frequencies," Laser & Photonics Reviews **9**, 83–90 (2015).
[33]Y. Zhang and Z. Han, "Spoof surface plasmon based planar antennas for the realization of terahertz hotspots," Scientific Reports **5**, 18606 (2015).
[34]Z. Han, Y. Zhang, and S. I. Bozhevolnyi, "Spoof surface plasmon-based stripe antennas with extreme field enhancement in the terahertz regime," Opt. Lett. **40**, 2533–2536 (2015).
[35]C. R. Williams, S. R. Andrews, S. Maier, A. Fernández-Domínguez, L. Martín-Moreno, and F. García-Vidal, "Highly confined guiding of terahertz surface plasmon polaritons on structured metal surfaces," Nature Photonics **2**, 175–179 (2008).
[36]A. J. Huber, F. Keilmann, J. Wittborn, J. Aizpurua, and R. Hillenbrand, "Terahertz near-field nanoscopy of mobile carriers in single semiconductor nanodevices," Nano letters **8**, 3766–3770 (2008).
[37]N. Sulollari, J. Keeley, S. Park, P. Rubino, A. D. Burnett, L. Li, M. C. Rosamond, E. H. Linfield, A. G. Davies, J. E. Cunningham, *et al.*, "Coherent terahertz microscopy of modal field distributions in micro-resonators," APL Photonics **6** (2021).
[38]L. Thomas, T. Hannotte, C. N. Santos, B. Walter, M. Lavancier, S. Eliet, M. Faucher, J.-F. Lampin, and R. Peretti, "Imaging of thz photonic modes by scattering scanning near-field optical microscopy," ACS Applied Materials & Interfaces **14**, 32608–32617 (2022).
[39]X. Guo, X. He, Z. Degnan, C.-C. Chiu, B. C. Donose, K. Bertling, A. Fedorov, A. D. Rakić, and P. Jacobson, "Terahertz nanospectroscopy of plasmon polaritons for the evaluation of doping in quantum devices," Nanophotonics **12**, 1865–1875 (2023).
[40]V. Pistore, L. Viti, C. Schiattarella, Z. Wang, S. Law, O. Mitrofanov, and M. S. Vitiello, "Holographic nano-imaging of terahertz dirac plasmon polaritons topological insulator antenna resonators," Small , 2308116 (2023).
[41]V. Pistore, L. Viti, C. Schiattarella, E. Riccardi, C. S. Knox, A. Yagmur, J. J. Burton, S. Sasaki, A. G. Davies, E. H. Linfield, J. R. Freeman, and M. S. Vitiello, "Terahertz plasmon polaritons in large area bi2se3 topological insulators," Advanced Optical Materials **n/a**, 2301673, https://onlinelibrary.wiley.com/doi/pdf/10.1002/adom.202301673.
[42]M. C. Giordano, S. Mastel, C. Liewald, L. L. Columbo, M. Brambilla, L. Viti, A. Politano, K. Zhang, L. Li, A. G. Davies, *et al.*, "Phase-resolved terahertz self-detection near-field microscopy," Optics express **26**, 18423–18435 (2018).
[43]P. Achmari, A. M. Siddiquee, G. Si, J. Lin, B. Abbey, and S. Kou, "Investigating the probe-tip influence on imaging using scanning near-field optical microscopy," OSA Continuum **4**, 1143–1154 (2021).
[44]A. García-Etxarri, I. Romero, F. J. G. de Abajo, R. Hillenbrand, and J. Aizpurua, "Influence of the tip in near-field imaging of nanoparticle plasmonic modes: Weak and strong coupling regimes," Physical Review B **79**, 125439 (2009).
[45]B. Hecht, H. Bielefeldt, L. Novotny, Y. Inouye, and D. W. Pohl, "Local excitation, scattering, and interference of surface plasmons," Phys. Rev. Lett. **77**, 1889–1892 (1996).